Computational Methods Elucidate Consequences of Mutations and Post-translational Modifications on Troponin I Effective Concentration to Troponin C

Austin M. Cool and Steffen Lindert*

Read Online

ACCESS | Metrics & More | Article Recommendations | SI Supporting Information

ABSTRACT: Ca^{2+} binding to cardiac troponin C (cTnC) causes a conformational shift that exposes a hydrophobic patch ($cTnC_{HP}$) for binding of the cTnI switch peptide ($cTnI_{SP}$), ultimately resulting in contraction of the heart. The inhibitory peptide ($cTnI_{IP}$), attached at the N-terminal end of the $cTnI_{SP}$, serves as a tether for the $cTnI_{SP}$ to the rest of the troponin complex. Due to this tethered nature, the $cTnI_{SP}$ remains within proximity of the hydrophobic patch region, resulting in the $cTnC_{HP}$ experiencing an elevated "effective concentration" of the $cTnI_{SP}$. Mutations to the $cTnI_{IP}$ region have been hypothesized to cause disease by affecting the ability of the $cTnI_{SP}$ to "find" the hydrophobic patch, resulting in alterations to the heart's ability to contract normally. We tested this hypothesis using molecular dynamics (MD) simulations of the troponin complex using a model that contained all three subunits of troponin: C, I, and T. We developed methods that allowed us to quantitatively measure the effective concentration of the $cTnI_{SP}$ from the simulations. A significant reduction in the $cTnI_{SP}$ effective concentration was observed when the $cTnI_{IP}$ was removed from the system, showcasing the importance of a tethered $cTnI_{SP}$. Through accelerated MD methods, we proposed the minimum effective concentration of a tethered $cTnI_{SP}$ to be approximately 21 mM. Modification of the $cTnI_{IP}$ via PKC-mediated phosphorylation of T143 was shown to significantly increase the estimated effective concentration of $cTnI_{SP}$, help the $cTnI_{SP}$ find the $cTnC_{HP}$ more effectively, and maintain the relative shape of the $cTnI_{IP}$ when compared to the native model. All of these data indicate that pT143 may be able to help promote binding of $cTnI_{SP}$ to the $cTnC_{HP}$. We then tested six mutations within the $cTnI_{IP}$ region that are known cTnC Ca^{2+}-sensitizing mutations and have been linked with cardiomyopathy. We did not observe a significant reduction in the effective concentration upon the introduction of these mutations; however, we did observe increased variability in the flexibility and dynamics of the $cTnI_{IP}$ region when compared to native. Our observations led us to hypothesize that the mechanism by which these cardiomyopathic mutations affect Ca^{2+} sensitivity is by altering the off rate of $cTnI_{SP}$ from the hydrophobic patch.
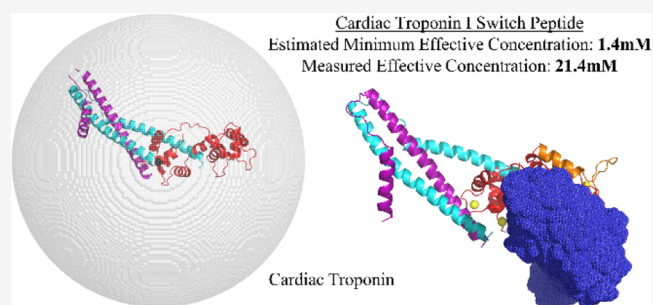
INTRODUCTION

The cardiac troponin complex (cTn) is responsible for modulating the interaction between myosin and actin necessary for muscle contraction.[1] cTn is made up of three subunits: Ca^{2+} binding subunit (cTnC), inhibitory subunit (cTnI), and tropomyosin-binding structural subunit (cTnT) that anchors the complex to the thin filament. Although there are four EF-hand Ca^{2+} binding sites in cTnC, only Ca^{2+} binding to site II regulates cardiac muscle contraction. When Ca^{2+} binds to this site, it causes a conformational shift within the N-terminal region of cTnC that exposes a hydrophobic patch ($cTnC_{HP}$, residues 20, 23, 24, 26, 27, 36, 41, 44, 48, 57, 60, 77, 80, and 81). This patch promotes binding of the cTnI switch peptide ($cTnI_{SP}$, residues 149−164), removing the C-terminal end of cTnI from its binding site on actin, and allowing myosin to interact with actin for muscle contraction.[2] Differences between the Ca^{2+} bound and unbound structures can be seen in Figure 1. The sequence directly N-terminal of

the $cTnI_{SP}$ is the largely unstructured inhibitory peptide ($cTnI_{IP}$, residues 137−148) that essentially acts as a tether for the $cTnI_{SP}$ to the rest of the cTn complex.

Cardiomyopathies are a collection of diseases that can thicken, stiffen, or thin out the heart muscle, which can lead to heart failure or sudden cardiac death.[3] Hypertrophic cardiomyopathy (HCM) is characterized by increased thickness of the interventricular septum and decreased left ventricular chamber volume, leading to the impaired diastolic function of the heart.[4] HCM affects 1 out of 500 people with more than 70% of cases being familial. Restrictive cardiomy-
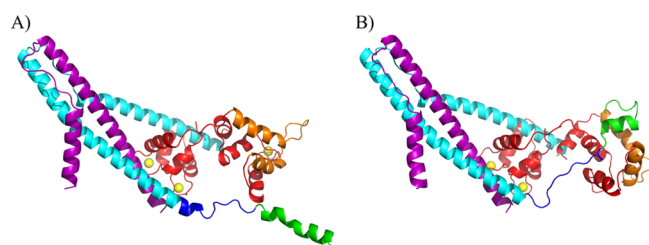
Figure 1. Ribbon representation of cardiac troponin. (A) Ca^{2+}-free, $cTnI_{SP}$-unbound, cardiac troponin (PDB: 6KN7, chains a, b, and c). (B) Ca^{2+}-bound, $cTnI_{SP}$-bound, cardiac troponin (PDB: 6KN8, chains a, b, and c). cTnT is shown in purple, cTnC is shown in red, helices that line the $cTnC_{HP}$ are shown in orange, the IT arm of cTnI is shown in cyan, with the $cTnI_{IP}$ in dark blue and the $cTnI_{SP}$ in green, and Ca^{2+} ions added by Autodock Vina are shown in yellow.

opathy (RCM) is a rarer disease state, characterized by impaired ventricular filling and a decreased diastolic volume. The prognosis for RCM is worse than HCM given that of individuals identified with RCM, 10% die by age 19 and 50% die before age 35.[5] HCM and RCM mutations have been identified within all subunits of cTn and have been experimentally shown to cause a shift in the Ca^{2+} sensitivity to site II of cTnC.[5]

How exactly cardiomyopathic mutations outside of the Ca^{2+} binding site of cTnC can cause a shift in Ca^{2+} sensitivity to this site has been the focus of intense research.[6−18] A previous study by Siddiqui et al.[19] proposed that the availability of the $cTnI_{SP}$ to the $cTnC_{HP}$ may be one explanation to the variability in Ca^{2+} sensitivity. It was suggested that due to the tethered nature of the $cTnI_{SP}$ via the $cTnI_{IP}$, the $cTnC_{HP}$ experiences an elevated effective concentration of $cTnI_{SP}$. During traditional molecular dynamics (MD) simulations of the cTn complex, a study by Dvornikov et al. observed a significant reduction in contacts between the residue cTnI 145 and cTnC residues E56, E59, and E63 when the R145W RCM or T143E phosphomimic mutations were present.[15] Given that cTnC has been shown to have a higher sensitivity for Ca^{2+} when $cTnI_{IP}$ is tethered to the complex, in addition to the observed reduction of contacts between $cTnI_{IP}$ and cTnC observed in MD simulations, we hypothesized that alterations to the $cTnI_{IP}$ region may change the effective concentration, and therefore, the Ca^{2+} sensitivity.

The focus of this study was to quantify how the $cTnI_{IP}$ works to help the $cTnI_{SP}$ "find" the $cTnC_{HP}$ and potentially elucidate a mechanism. A recent structure proposed by cryo-EM studies from Yamada et al.[20] was selected as the starting model for MD simulations as it contained cTn within its natural environment of the thin filament. A cartoon representation of this model, created using Illustrate,[21] can be seen in Figure S1 in Supporting Information. We investigated six different mutations within the $cTnI_{IP}$ region that have been associated with cardiomyopathy: L141Q, L144P, L144Q, R145G, R145Q, and R145W. The L144Q and R145W mutations have been associated with RCM, while the other four have been associated with HCM.[5] All mutations have been experimentally shown to increase Ca^{2+} sensitivity,[22,23] with the RCM mutations causing a more drastic increase in Ca^{2+} sensitivity than HCM.[24] In addition to these cardiomyopathic mutations, we also performed simulations with a phosphorylated cTnI pT143. The introduction of this phosphothreonine had conflicting reported evidence on Ca^{2+}

sensitivity effects but has been shown to disrupt the cooperativity of activation and decrease the relaxation rate.[25]

We geometrically investigated the $cTnI_{SP}$ effective concentration by developing a computational methodology to explicitly measure it from molecular simulations. This method can effectively estimate the volume sampled by atoms within the $cTnI_{SP}$ throughout the course of all our simulations. This allowed us to test how alterations to the $cTnI_{IP}$ region affected the effective concentration. Our results showed virtually no change in the effective concentration for any of the cardiomyopathic mutations, but we did observe a significant increase in the effective concentration for the phosphothreonine models.

◼ METHODS

Model Preparation. The starting model representing cTn was extracted from PDB entry 6KN7, a cryo-EM structure, representing a Ca^{2+}-free, $cTnI_{IP}$ unbound, and $cTnI_{SP}$ tethered conformation of the complex. Residues extracted from PDB 6KN7 included cTnT 199−272 (chain a), cTnI 41−166 (chain b), and cTnC 2−161 (chain c). To generate a Ca^{2+}-bound model, Ca^{2+} ions were added to site II and the two sites in the C-terminal region of cTnC using AutoDock Vina.[26] The same process was followed to create a Ca^{2+}-bound, $cTnI_{SP}$-bound, and $cTnI_{SP}$-tethered model using the PDB entry 6KN8. The addition of Ca^{2+} ions via AutoDock Vina to these structures was a necessary step as neither 6KN7 nor 6KN8 contained the positions of Ca^{2+} ions. Standard protonation states for residues contained within the Ca^{2+}-binding domains of cTnC were used as it has been shown that these residues are highly resistant to alterations in their protonation state.[27] A Ca^{2+}-bound model with an unbound and untethered $cTnI_{SP}$ was created by deleting the $cTnI_{IP}$ residues 137−148 from the Ca^{2+}-bound, $cTnI_{SP}$-unbound, and $cTnI_{SP}$-tethered starting model. Cardiomyopathic mutation models were generated using the Ca^{2+}-bound, $cTnI_{SP}$-unbound, and $cTnI_{SP}$-tethered starting model using the mutagenesis wizard function available in PyMOL.[28] A phosphorylated version of each $cTnI_{SP}$ tethered model was then created using the same Ca^{2+}-bound, $cTnI_{SP}$-unbound, and $cTnI_{SP}$-tethered starting model using the PyTMs[29] plug-in available in PyMOL.

MD Simulations and Enhanced Sampling Methods. For the MD simulations, the models were solvated with explicit TIP3W water molecules, and NaCl counterions were added to neutralize the entire system and bring it to a final salt concentration of 150 mM. This system was restrained, followed by the energy of the water molecules and protein being minimized over two separate subsequent 10,000 step minimizations, with a step size of 2 fs. The restraints were then removed in an initial equilibration of 190,000 steps, with a final equilibration of 10,000 steps occurring production run conditions. All preparation steps and MD simulations were conducted using NAMD 2.13[30] with the CHARMM36 force field.[31] The MD simulations were conducted using an *NPT* ensemble at 310 K with Langevin temperature and pressure dampening. All bonds with hydrogen were constrained using the ShakeH algorithm which allowed for a 2 fs timestep, with structures being saved every 2 ps. The simulations were carried out on the Owens Cluster of the Ohio Supercomputer Center[32] using 28 processors on one node, for 50,000,000 steps, resulting in 100 ns simulations for each system. After the simulation was completed, the system was stripped of all water molecules and Na^+/Cl^- ions. Then, each saved structure was

aligned to the first frame to create a new DCD file. This resulting DCD file was then used for all analysis methods.

All preparation steps for accelerated MD[33] (AMD) mimicked those of the traditional MD preparation steps and were performed using NAMD 2.13 with the CHARMM36 force field. Additional parameters for running AMD included applying the boost energy to the dihedral potential of the system. The threshold energy (E) and acceleration factor (α) were applied after they were determined to be 5437 and 408.8 kcal/mol, respectively, using data from an equilibrated traditional MD simulation of the cTn complex. The resulting DCD files were stripped of waters and aligned, as described above. Brownian dynamics (BD) simulations were performed using BrownDye,[34] with an electrostatic grid input being generated using APBS.[35] Normally, BrownDye is employed to observe the association between two entities, whether it be enzyme−substrate or protein−peptide.[34] BrownDye allows the user to input criteria that would tell the program that a "reaction" has occurred if the substrate/peptide was to occupy a given space. However, we wanted to employ BD for enhanced sampling of the conformational space available to the switch peptide, and thus, we did not want a reaction to occur. Hence, we have chosen a "phantom" atom approach to allow the $cTnI_{SP}$ to "escape" during every trajectory. This allowed the $cTnI_{SP}$ to essentially sample as much volume as possible throughout the simulation time. This approach was carried out by creating two "phantom" OD1 atoms within the $cTnC_{HP}$ and designating that for a reaction to occur, the CA atoms of residues cTnI 149 and 164 must be within 1.0 Å of these phantom atoms. Since this was impossible to occur during the simulation, the $cTnI_{SP}$ continued to sample space for the desired steps in the trajectory unless the $cTnI_{SP}$ "escaped" the cTn complex. 5000 trajectories were created with 1,000,000 maximum steps per trajectory, and the coordinates of the $cTnI_{SP}$ were saved every 10 steps.

Effective Concentration Measurements Using VECA. For each of the MD and AMD simulations, 50,000 frames were created over the course of 100 ns (1 frame every 2 ps). For analysis purposes, we extracted every fourth frame from the trajectories, totaling 12,500 PDB files, or one frame every 8 ps. For the BD simulations, every 25th frame from the trajectories was extracted for analysis. The effective concentration of the $cTnI_{SP}$ was directly measured for all these simulations using a method we refer to as "volume estimation using cube approximation" or VECA. It was implemented as an in-house python script where a sphere with a given radius is generated using 1 Å × 1 Å × 1 Å cubes. The center of this sphere is the average position of the CA atom of cTnI 136, the last residue before the $cTnI_{IP}$ region that serves as an anchor for the tether. For all atoms in the $cTnI_{SP}$ region (residues 149−164) in every extracted frame of the simulation being measured, the cubes that these atoms occupy are marked within the sphere. To account for the size of the atoms, we marked six additional points within the sphere in the positive and negative x-, y-, z-directions using the following values for covalent radii: hydrogen (0.31 Å), carbon (0.71 Å), oxygen (0.66 Å), nitrogen (0.71 Å), sulfur (1.05 Å), and phosphorous (1.07 Å).[36] The creation of these additional points helped better account for atom size and sample cubes that may have otherwise been missed with just marking the center position of the atom. After all frames of a simulation had been analyzed, the total number of uniquely sampled cubes was totaled to yield a sampled volume in Å[3]. This volume was converted into

liters and subsequently used to determine an effective concentration assuming one molecule of $cTnI_{SP}$ in the volume sampled. A detailed example of this calculation can be seen in the Results and Discussion section.

Trajectory Analysis of Simulations. For each extracted frame of the MD simulations, the distance between the $cTnI_{SP}$ and $cTnC_{HP}$ was measured by determining the average position of cTnI C-α atoms in residues 149−164 and calculating the distance of the average position of those cTnI atoms to cTnC residues 20, 23, 24, 26, 27, 36, 41, 44, 48, 57, 60, 77, 80, and 81. These cTnC residues were selected to match those in a previous study of the exposure of the hydrophobic patch.[37] The radius of gyration (R_g) for the $cTnI_{IP}$ was calculated for each frame and then graphed as a function of time over the course of the simulation. The formula used to calculate the radius of gyration was: $R_g = \sqrt{\frac{\sum_{i=1}^{N} m_i r_i^2}{M}}$, where N = total number of atoms of the $cTnI_{IP}$; M = total mass of the $cTnI_{IP}$; m_i = mass of atom i; and r_i = distance between center of mass of the $cTnI_{IP}$ and atom i.

■ RESULTS AND DISCUSSION

Geometric Estimation Determined Low-Micromolar Minimum Effective $cTnI_{SP}$ Concentration. We first geometrically estimated the maximum volume that a tethered $cTnI_{SP}$ could theoretically sample. For infinitely efficient sampling and neglecting any steric hindrance by the remainder of the troponin complex, this would set a lower limit to the effective switch peptide concentration. Based on geometric arguments, we assumed that there will be one molecule of $cTnI_{SP}$ within a volume defined by a sphere with a radius equal to the maximum possible length of the stretch of amino acids involved in the $cTnI_{IP}$ and $cTnI_{SP}$ regions. We further assumed that the $cTnI_{IP}$ region (12 residues, 137−148) can take on a fully extended conformation with a contour length per residue of 3.5 Å,[38] and that the $cTnI_{SP}$ region (16 residues, 149−164) will remain in a helical confirmation with a rise per residue of 1.5 Å,[39] as observed in PDB 6KN7. Under these assumptions, the minimum effective concentration can be calculated as follows

$$\text{Max radius} = (12 \text{ residues} \times 3.5 \text{ Å})$$
$$+ (16 \text{ residues} \times 1.5 \text{ Å})$$
$$= 66 \text{ Å}$$

$$\text{Max volume} = \frac{4}{3}\pi(66 \text{ Å})^3 = 1{,}204{,}260 \text{ Å}^3 \times \frac{\text{m}^3}{10^{30} \text{ Å}^3}$$
$$\times \frac{1000 \text{ L}}{1 \text{ m}^3} = 1.20 \times 10^{-21} \text{ L}$$

$$\text{Moles} = \frac{1 \text{cTnIsp}}{6.02 \times 10^{23} \frac{\text{cTnIsp}}{\text{mol}}}$$

$$\text{Min. eff. concentration} = \frac{\text{moles}}{\text{max volume}} = 1.38 \text{ mM}$$

Therefore, in the limit of infinitely efficient sampling and neglecting steric hindrance by cTn, a tethered $cTnI_{SP}$ would be able to sample all the available space in a sphere with a 66 Å radius, leading to an effective concentration of 1.38 mM. Our estimated minimum effective concentration for a $cTnI_{SP}$ is comparable to the 3 mM estimated effective concentration

proposed by Siddiqui et al.[19] A representation of the maximum volume, available to the tethered $cTnI_{SP}$, in the context of the cTn complex is shown in Figure 2. This value is an estimation
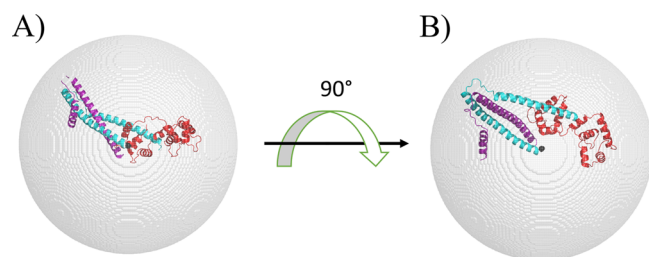
Figure 2. Representation of the VECA method. (A) "Side" view (same angle as shown in Figure 1) and (B) "top-down" view of the cTn complex within a sphere of 66 Å created using the VECA method. The black dot in the middle of the sphere is the position of the CA atom of TnI 136.

of the total amount of the space available to the $cTnI_{SP}$ and does not account for the volume occupied by the remaining cTn residues in that sphere or for unrealistic backbone torsional angles within the $cTnI_{IP}$ residues that could potentially prevent the $cTnI_{SP}$ from sampling certain parts of space centered around the anchor residue cTnI 136. When creating a sphere of 66 Å radius using the VECA method, the representative sphere comprised 1,204,466 empty cubes, a 206 $Å^3$ (0.02%) difference from the theoretical volume calculated above. Likewise, the volume of the cTn complex without the $cTnI_{IP}$ or $cTnI_{SP}$ was determined to be 16,862 $Å^3$. By removing the unsampleable space occupied by the cTn complex, the maximum volume available to the $cTnI_{SP}$ was then 1,187,604 $Å^3$, thus leading to a minimum effective concentration of 1.40 mM.

BD Simulation Verified VECA Method and Determined Minimum Effective Concentrations of $cTnI_{SP}$. We performed a BD simulation using a Ca^{2+}-bound and $cTnI_{SP}$-unbound and untethered model to test our VECA method for accuracy and to determine a minimum effective concentration of an untethered $cTnI_{SP}$. If enough trajectories are simulated, theoretically the $cTnI_{SP}$ should be able to sample every cube within the 66 Å radius sphere that does not contain the cTn complex. The results from the BD simulation determined that the $cTnI_{SP}$ sampled a volume of 1,187,604 $Å^3$ within the sphere, which is 100% of the sampleable space available to the $cTnI_{SP}$, resulting in an estimated effective concentration of 1.40 mM. This value would therefore represent the lowest effective concentration for the $cTnI_{SP}$ given the volume of the cTn complex is unsampleable and restricting the $cTnI_{SP}$ within the 66 Å radius. This evidence shows that our VECA method is efficient at representing the 66 Å sphere, and it can accurately measure sampled volumes during a simulation. If the radius restriction is removed from the BD volume estimation, the $cTnI_{SP}$ is essentially unrestrained within the simulation. Troponin molecules are spaced out approximately 386.4 Å from each other along the thin filaments.[20] When the VECA calculation was performed in a relatively large cube with 300 Å sides to represent this physiological spacing (with a maximum volume of 27,000,000 $Å^3$), we observed a total volume of 12,017,637 $Å^3$ sampled during the BD simulations. This correlated to a 10-fold increase in the volume sampled compared to when the evaluation was limited to a sphere of radius 66 Å. This allowed us to estimate the minimal effective

concentration of the untethered $cTnI_{SP}$ to be 0.14 mM. Hence, we estimate that the $cTnI_{IP}$ tether increases the $cTnI_{SP}$ effective concentration by at least an order of magnitude.

MD Simulations Showed Significant Reduction of the Effective Concentration When $cTnI_{IP}$ Tether Is Removed. After using BD and geometric considerations to establish that the VECA method could accurately estimate the $cTnI_{SP}$ effective concentration, we measured the effective concentration of tethered and untethered $cTnI_{SP}$ models (both Ca^{2+} bound) during 100 ns MD simulations. Using the restriction of a 66 Å radius from TnI 136, the average effective concentration for the tethered models was determined to be 29.7 ± 5.5 mM, whereas the effective concentration for the untethered models was determined to be 13.4 ± 8.0 mM. Standard deviations were calculated based on 25 trials for each system. These data correspond to volumes sampled by the $cTnI_{SP}$ of 55,930 and 123,964 $Å^3$, respectively. It is physically impossible for the tethered $cTnI_{SP}$ simulation to have the $cTnI_{SP}$ extend beyond the 66 Å radius; however, it did occur within the simulations with an untethered $cTnI_{SP}$. When the 66 Å restriction was removed from the VECA method, we determined the untethered $cTnI_{SP}$ to experience an effective concentration of 9.8 ± 9.0 mM, which correlated to an average sampled volume of 169,503 $Å^3$. The large difference between observed tethered and untethered effective concentrations within only 100 ns, a short time compared to that of contraction, quantifies the importance of the $cTnI_{IP}$ tether for the function of the cTn complex. Figure 3 illustrates the
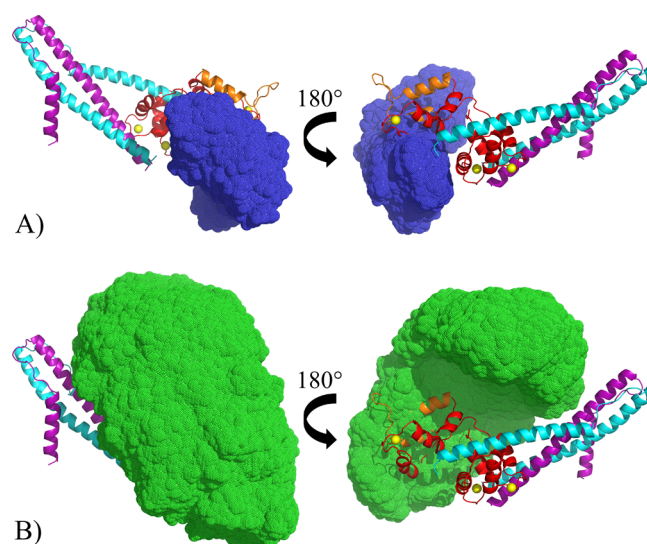
Figure 3. Representations of the space sampled using the VECA method. (A) Space sampled by a tethered switch peptide with a volume of 55,146 $Å^3$. (B) Space sampled by an untethered switch peptide with an estimated volume of 141,528 $Å^3$. All figures were made using the most representative trial for each model, determined by having the closest measured effective concentration to the model's average.

difference between the space sampled by each of these models within 100 ns. These figures were generated using the most representative trials, which exhibited the closest measured effective concentration to the model average. Figure 3 shows that the untethered switch peptide was free to sample space all around the cTn complex, whereas the tethered switch peptide

stayed within the general vicinity of the N-terminal region of cTnC.

AMD Simulations Further Quantitatively Demonstrated Importance of Tethered cTnI$_{SP}$. To explore the role of limited sampling in our estimations of effective cTnI$_{SP}$ concentration from MD simulations and to probe the minimum effective concentration of a tethered cTnI$_{SP}$, we performed AMD on the Ca^{2+}-bound and cTnI$_{SP}$-unbound, tethered model of cTn. These simulations were run in triplicate for 100 ns. Using this method, we calculated the effective cTnI$_{SP}$ concentration to be 21.4 ±1.9 mM, with an average volume of 77,622 Å^3. Figure 4 shows volume sampled
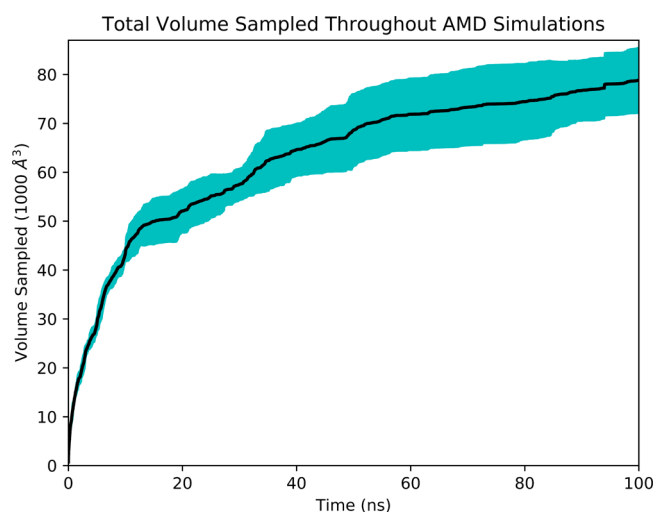
Figure 4. Volume sampled by AMD trajectories averaged across the three trials over the course of the simulation. Standard deviation is shown as the shaded region around the average.

averaged across the three trials over the course of the simulation. The cumulative volume sampled seemed to be plateauing by the end of the 100 ns simulations, indicating that 21.4 mM may be a near-convergent estimation of the actual effective concentration for a tethered switch peptide. This quantitatively demonstrated that the existence of the tether precludes sampling of large parts of the volume that would be accessible if the cTnI$_{SP}$ was not being tethered to the cTn complex via the cTnI$_{IP}$.

cTnI$_{IP}$ Cardiomyopathic Mutations Showed No Significant Change to the Estimated Effective Concentration. With the importance of a tether being established, the effects of altering the natural state of this tether were tested. First, the effective concentration of a tethered cTnI$_{SP}$ during 100 ns MD simulations was measured for six cardiomyopathic mutations in the cTnI$_{IP}$ region: R141Q, L144P, L144Q, R145G, R145Q, and R145W. The calculated effective concentrations are listed in Table 1, with the standard deviations calculated based on three trials for each model. We did not observe any significant difference in effective concentrations for the cardiomyopathic mutations. To analyze differences in cTnI$_{SP}$–cTnC interactions, we calculated the distance between the cTnI$_{SP}$ and cTnC$_{HP}$, as described in the Methods section, as a function of time over the simulation (Figure 5). Both panels of Figure 5 contain data for the trials that simulated a model of Ca^{2+}-bound, cTnI$_{SP}$-tethered, and cTnI$_{SP}$-bound cTn complex made from PDB 6KN8. These simulations were performed to establish a baseline minimum

Table 1. Effective Concentration for Native and Mutated Models

cTn model	effective concentration (mM)
native	29.7 ± 5.5
R141Q	26.0 ± 5.1
L144P	29.7 ± 4.4
L144Q	28.3 ± 4.3
R145G	22.8 ± 5.3
R145Q	30.0 ± 5.6
R145W	30.2 ± 4.3

distance of these two regions for a cTnI$_{SP}$ that was bound to the cTnC$_{HP}$. This helped put into perspective the relative distances calculated for the cTnI$_{SP}$-unbound models. We observed that although there was no significant difference in the amount of volume sampled over time, three HCM mutations (R141Q, L144P, and R145G) preferentially sampled space distant from the N-terminal region of cTnC compared to the native 6KN7 model. The other three mutations (R145Q, L144Q, and R145W) did not impact the distance of the cTnI$_{SP}$ to the N-terminal region of cTnC compared to the native.

Interhelical Angle Analysis Revealed No Significant Opening Events during MD Simulations. The interhelical angle between cTnC helices A and B has been shown to be a good indicator of when the cTnC$_{HP}$ is exposed or "open."[40] Using a cutoff of 105°, where above this cutoff would indicate a closed conformation and below would indicate an open conformation, during the Ca^{2+}-bound, cTnI$_{SP}$-unbound, cTnI$_{SP}$-tethered MD simulations, we were unable to see any significant opening events. Given the relatively short timescale of these simulations compared to the estimated timescale of hydrophobic patch opening,[41−44] this was not unexpected, but it did inhibit our ability to see a complete shift from an unbound cTnI$_{SP}$, closed patch model to a cTnI$_{SP}$-bound, open patch model. The apparent asymptote in the cTnI$_{SP}$–cTnC$_{HP}$ distance graphs (Figure 5A) around 14 Å arose from the inability of the cTnI$_{SP}$ in the unbound models to bind to the cTnC$_{HP}$ since it never opened throughout the MD simulations. Without this opening event, 14 Å was the closest possible distance of the cTnI$_{SP}$ to the cTnC$_{HP}$. A model of the cTnI$_{SP}$ bound to a closed cTnC$_{HP}$ can be seen in Figure S2 of Supporting Information. During the time in MD simulations where the distance is shown to be in this asymptotic range (for R145Q), the cTnI$_{SP}$ was essentially just interacting with the N-terminal region of cTnC, potentially primed to bind to the cTnC$_{HP}$ if it were to open.

Analysis of Distance between cTnI 145 and cTnC E56/E59/E63. To discern differences in interactions between the cTnI$_{SP}$ and the N-terminal domain of cTnC, we evaluated the distance between the residue cTnI 145 and cTnC residues E56, E59, and E63. A previous study observed a decrease in the interaction between these residue pairs when comparing native and R145W models during MD simulations.[15] The results can be seen in Table 2. The only model to experience a notable increase in residue–residue distance across all three pairings was the R145G mutation. We observed slight decreases in residue–residue distances across all three pairings for the L144P mutation. However, in both cases the ranges of the standard deviations overlapped with that of the native data, preventing us from concluding that these differences were significant enough to investigate further. These data, combined
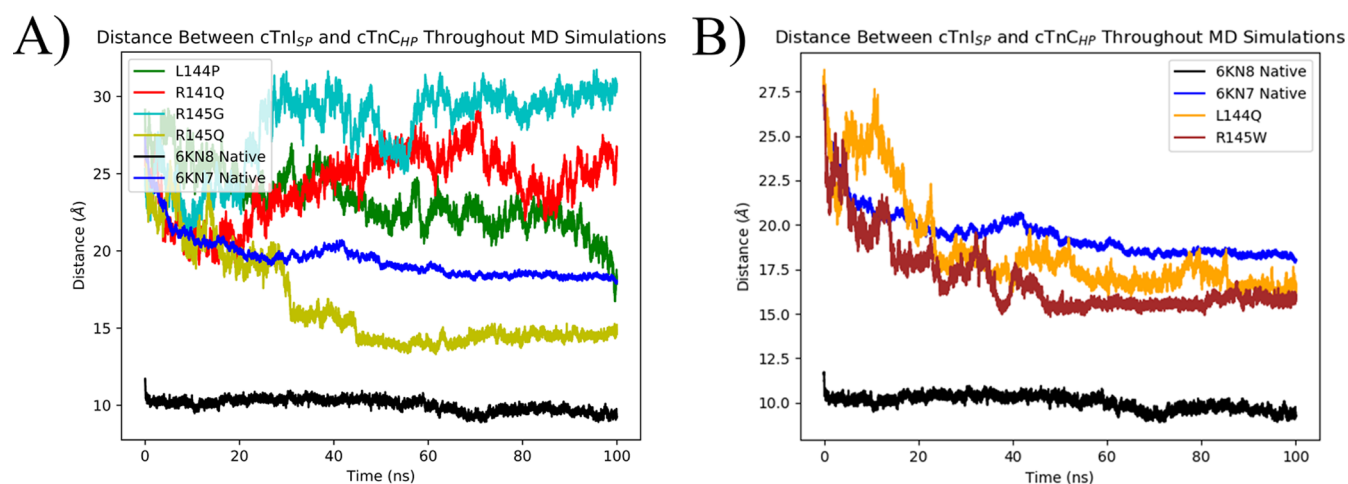
Figure 5. Distance between the cTnI$_{SP}$ and cTnC$_{HP}$ over the course of the traditional MD simulations of Ca^{2+} bound, cTnI$_{SP}$ tethered, and cTnI$_{SP}$ unbound. (A) Data for four HCM mutations and (B) data for two RCM mutations. Both graphs contain the 6KN7 and 6KN8 native data.

Table 2. Average Distance between cTnC 56/59/63 and cTnI 145[a]

cTnC residue	metric	model						
		native	R141Q	L144P	L144Q	R145G	R145Q	R145W
E56	avg. distance (Å)	15.7 ± 3.2	15.2 ± 4.5	12.7 ± 4.0	17.2 ± 1.6	21.1 ± 4.9	16.7 ± 1.3	17.7 ± 5.1
E59	avg. distance (Å)	19.4 ± 3.7	18.4 ± 4.5	16.8 ± 4.7	21.4 ± 1.6	23.6 ± 5.6	21.3 ± 1.4	21.6 ± 4.8
E63	avg. distance (Å)	24.5 ± 3.3	24.1 ± 4.5	22.3 ± 4.5	26.5 ± 1.3	27.0 ± 6.8	25.5 ± 1.5	25.5 ± 3.3

[a]All averages and standard deviations are calculated over all trials performed for each system.

with our effective concentration evaluation, would suggest the mechanism by which the cTnI$_{IP}$ aids the cTnI$_{SP}$ in finding the hydrophobic patch involves more than one residue within the cTnI$_{IP}$ region, and that a singular mutation may not be enough to significantly disrupt this process. The only mutation that caused a notable impact, as measured by these two metrics, was R145G.

Radius of Gyration Calculation Showed Increased Variability in cTnI$_{IP}$ in Most Cardiomyopathic Models. We further analyzed the dynamics of the cTnI$_{IP}$ region by measuring its radius of gyration (R_g) as a function of time throughout the cTnI$_{SP}$-unbound, cTnI$_{SP}$-tethered MD simulations (Figure S2). Given that there was no significant change in the estimated effective concentration, we did not expect to observe a higher R_g for the mutated models. However, we did observe an increased variability in R_g in the RCM mutations, indicating that the mutated cTnI$_{IP}$ region was less stable than the native sequence. A similar observation was made for the HCM mutations, except for the R145Q mutant, which exhibited a native-like trend. The R145G mutation experienced the largest variability in radius of gyration, as well as the largest observed R_g values for any of the models. This was not surprising as this mutation was shown to have sampled the most space throughout the simulations (Table 1). Interestingly, the 6KN8 model that contained a cTnI$_{SP}$ bound to an open cTnC$_{HP}$ exhibited the largest R_g values for any of the models. Inspection of the cTnI$_{IP}$ conformation, as shown in Figure 1B, reveals that the entire cTnI$_{IP}$ region is extended with no apparent secondary structure, whereas in the unbound conformation (6KN7, Figure 1A), residues 137−143 have helical character, leading to a decrease in R_g, as compared to 6KN8. Elucidation of the timescale of the elongation of the cTnI$_{IP}$ could be an endeavor of a future project as it was not observed in any of our MD simulations.

cTnI Phosphothreonine 143 Stabilized the cTnI$_{IP}$ Region Causing an Increased Effective Concentration. Shifting the focus from mutations to post-translational modifications, we measured the sampled volume, and hence the effective concentration, for the cTnI phosphothreonine 143 (pT143) cTnI$_{SP}$-tethered, cTnI$_{SP}$-unbound model. pT143 has conflicting experimental evidence on its mechanism[25] but is generally thought to decouple the activation of cardiac muscle and decrease the relaxation rate. A previous computational study used a phosphomimic mutation, T143E, and noticed decreased contacts between cTnI 145 and cTnC residues 56, 59, and 63, which would suggest a decrease in cooperativity.[15] Using the same analytical techniques as described for the cardiomyopathic mutations, we observed a significant increase in the effective concentration, an improved ability to find the cTnC, and similar R_g data when compared to the native simulations. pT143 simulations were determined to have an estimated cTnI$_{SP}$ effective concentration of 40.8 ± 4.6 mM, where the standard deviation was calculated from three trials. This effective concentration correlated to an average sampled volume of 40,714 Å^3. This was a significant decrease in the sampled volume and increase in the effective concentration from the 29.7 mM average for wild-type cTn. Figure S3 illustrates the data collected for the cTnI$_{SP}$ distance to the cTnC$_{HP}$ and R_g calculations. The pT143 modification facilitated the cTnI$_{SP}$ experience a shorter distance to the cTnC$_{HP}$ than the native unbound model. Furthermore, the R_g data mostly aligned with that of the native, leading us to conclude that the structure of this region remained largely unperturbed. Figure S5 shows a comparison between the conformations sampled by the native and pT143 simulations. During the pT143 simulation, the cTnI$_{SP}$ was more often in the position to bind the cTnC$_{HP}$ and mimicked the 6KN8 Ca^{2+}-bound, cTnI$_{SP}$-bound structure (Figure 1B).

Interestingly, we observed zero interactions between cTnI R145 and cTnC E56/E59/E63 throughout any of the three trials, an observation that aligned with previous experiments on the phenomenon, albeit with a T143E phosphomimic model rather than an actual phosphothreonine.[15] All this evidence suggested that pT143 does not induce any large structural changes to the cTnI$_{IP}$ region but does promote binding of the cTnI$_{sp}$ to the cTnC$_{HP}$.

Introducing cTnI Phosphothreonine 143 to cTnI$_{IP}$ Cardiomyopathic Models Did Not Increase the Effective Concentration. To see whether phosphorylation had a similar effect on the cardiomyopathic mutation models, we introduced pT143 to each of the mutated models and ran the same analyses previously described. We saw virtually no change in the effective concentration between the mutated phosphorylated and unphosphorylated models except a slight increase in the R141Q model (Figure 6). Previous experimental research
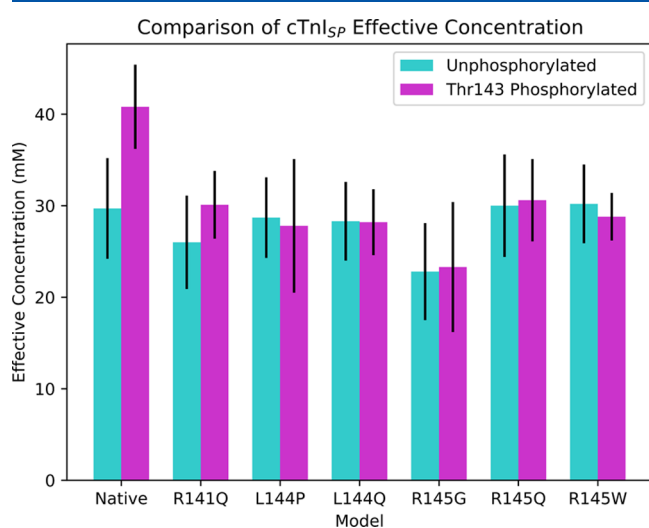
Figure 6. Comparison of measured cTnI$_{SP}$ effective concentrations in the unphosphorylated (blue) and pT143-modified state (purple).

has shown that pT143 is vastly reduced or does not occur when the R145W mutation is present,[15] possibly due to the binding motif required for PKC-mediated phosphorylation being disrupted by a mutation only two residues downstream of the target residue. This observation, coupled with our data, may suggest that pT143 is not possible for any of the tested cardiomyopathic mutations. Disruption of this phosphorylation process could therefore be a mechanism of disease caused by these mutations.

CONCLUSIONS

Through our MD simulations, we were able to quantify the effect of a tethered switch peptide in the cTn complex by using the in-house VECA method. As hypothesized, removing the tether vastly decreased the measured effective concentration of cTnI$_{SP}$ by allowing it to sample space that is not within the proximity of the cTnC$_{HP}$. This effect was observed in both classical MD and BD simulations. Through AMD simulations with a tethered cTnI$_{SP}$, we observed a plateauing of sampled space toward the end of the simulations, indicating that 21.4 mM may be a reliable estimate of the actual effective concentration of a tethered cTnI$_{SP}$. Modification of the cTnI$_{IP}$ via PKC-mediated phosphorylation of T143 was shown to significantly increase the estimated effective concentration of

cTnI$_{SP}$, help the cTnI$_{SP}$ find the cTnC$_{HP}$ more effectively, and maintain the relative shape of the cTnI$_{IP}$ when compared to the native model. All of these data indicate that pT143 may be able to help promote binding of cTnI$_{SP}$ to the cTnC$_{HP}$.

The mechanism by which cardiomyopathic mutations in the cTnI$_{IP}$ region cause disease remains unclear. Our studies indicated that they likely do not impact the effective switch peptide concentration meaningfully. R145G was the only studied mutation that caused a noticeable decrease in the measured cTnI$_{SP}$ effective concentration. R145-E56 contacts were unaffected by R141Q, slightly increased in L144 mutations, and significantly dampened by all R145 mutations. R145-E59 contacts were essentially knocked out by all mutations; however, these contacts were only observed around 5% of the time in native simulations. R145Q, L144Q, and R145W all showed an increased ability to help the cTnI$_{IP}$ "find" the cTnC$_{HP}$. R145Q was also observed to have the most native-like R_g throughout the simulations, whereas the other mutations had increased R_g or varying R_g. Our data do not support the hypothesis that the mechanism of disease caused by these mutations is predominantly based on altering the effective concentration of the cTnI$_{SP}$ to the cTnC$_{HP}$.

ASSOCIATED CONTENT

Supporting Information

The Supporting Information is available free of charge at https://pubs.acs.org/doi/10.1021/acs.jpcb.1c03844.

Cartoon representation of the cardiac thin filament, distance between cTnI$_{SP}$ and cTnC$_{HP}$, radius of gyration data for HCM/RCM mutations, data for distance between cTnI$_{SP}$ and cTnC$_{HP}$, R_g for the pT143 models, and ribbon representations of conformations assumed by native and pT143 troponin models (PDF)

AUTHOR INFORMATION

Corresponding Author

Steffen Lindert − *Department of Chemistry and Biochemistry, The Ohio State University, Columbus, Ohio 43210, United States;* orcid.org/0000-0002-3976-3473; Phone: 614-292-8284; Email: lindert.1@osu.edu; Fax: 614-292-1685

Author

Austin M. Cool − *Department of Chemistry and Biochemistry, The Ohio State University, Columbus, Ohio 43210, United States*

Complete contact information is available at:
https://pubs.acs.org/10.1021/acs.jpcb.1c03844

Notes

The authors declare no competing financial interest.

REFERENCES

(1) Marston, S.; Zamora, J. E. Troponin structure and function: a view of recent progress. *J. Muscle Res. Cell Motil.* **2020**, *41*, 71−89.

(2) Kobayashi, T.; Solaro, R. J. Calcium, thin filaments, and the integrative biology of cardiac contractility. *Annu. Rev. Physiol.* **2005**, *67*, 39−67.

(3) Richardson, P.; McKenna, W.; Bristow, M.; Maisch, B.; Mautner, B.; O'Connell, J.; Olsen, E.; Thiene, G.; Goodwin, J.; Gyarfas, I.; Martin, I.; Nordet, P. Report of the 1995 World Health Organization/International Society and Federation of Cardiology Task Force on the Definition and Classification of cardiomyopathies. *Circulation* **1996**, *93*, 841−842.

(4) Morimoto, S. Sarcomeric proteins and inherited cardiomyopathies. *Cardiovasc. Res.* **2008**, *77*, 659−666.

(5) Lu, Q. W.; Wu, X. Y.; Morimoto, S. Inherited cardiomyopathies caused by troponin mutations. *J. Geriatr. Cardiol.* **2013**, *10*, 91−101.

(6) Hamdani, N.; de Waard, M.; Messer, A. E.; Boontje, N. M.; Kooij, V.; van Dijk, S.; Versteilen, A.; Lamberts, R.; Merkus, D.; Dos Remedios, C.; Duncker, D. J.; Borbely, A.; Papp, Z.; Paulus, W.; Stienen, G. J.; Marston, S. B.; van der Velden, J. Myofilament dysfunction in cardiac disease from mice to men. *J. Muscle Res. Cell Motil.* **2008**, *29*, 189−201.

(7) Liu, B.; Lee, R. S.; Biesiadecki, B. J.; Tikunova, S. B.; Davis, J. P. Engineered troponin C constructs correct disease-related cardiac myofilament calcium sensitivity. *J. Biol. Chem.* **2012**, *287*, 20027−20036.

(8) Liu, B.; Lopez, J. J.; Biesiadecki, B. J.; Davis, J. P. Protein kinase C phosphomimetics alter thin filament Ca2+ binding properties. *PLoS One* **2014**, *9*, No. e86279.

(9) Liu, B.; Tikunova, S. B.; Kline, K. P.; Siddiqui, J. K.; Davis, J. P. Disease-related cardiac troponins alter thin filament Ca2+ association and dissociation rates. *PLoS One* **2012**, *7*, No. e38259.

(10) Nixon, B. R.; Thawornkaiwong, A.; Jin, J.; Brundage, E. A.; Little, S. C.; Davis, J. P.; Solaro, R. J.; Biesiadecki, B. J. AMP-activated protein kinase phosphorylates cardiac troponin I at Ser-150 to increase myofilament calcium sensitivity and blunt PKA-dependent function. *J. Biol. Chem.* **2012**, *287*, 19136−19147.

(11) Tardiff, J. C. Thin filament mutations: developing an integrative approach to a complex disorder. *Circ. Res.* **2011**, *108*, 765−782.

(12) Lindert, S.; Cheng, Y.; Kekenes-Huskey, P.; Regnier, M.; McCammon, J. A. Effects of HCM cTnI mutation R145G on troponin structure and modulation by PKA phosphorylation elucidated by molecular dynamics simulations. *Biophys. J.* **2015**, *108*, 395−407.

(13) Cheng, Y.; Lindert, S.; Oxenford, L.; Tu, A.-y.; McCulloch, A. D.; Regnier, M. Effects of Cardiac Troponin I Mutation P83S on Contractile Properties and the Modulation by PKA-Mediated Phosphorylation. *J. Phys. Chem. B* **2016**, *120*, 8238−8253.

(14) Cheng, Y.; Rao, V.; Tu, A.-y.; Lindert, S.; Wang, D.; Oxenford, L.; McCulloch, A. D.; McCammon, J. A.; Regnier, M. Troponin I Mutations R146G and R21C Alter Cardiac Troponin Function, Contractile Properties, and Modulation by Protein Kinase A (PKA)-mediated Phosphorylation. *J. Biol. Chem.* **2015**, *290*, 27749−27766.

(15) Dvornikov, A. V.; Smolin, N.; Zhang, M.; Martin, J. L.; Robia, S. L.; de Tombe, P. P. Restrictive cardiomyopathy troponin I R145W mutation does not perturb myofilament length-dependent activation in human cardiac sarcomeres. *J. Biol. Chem.* **2016**, *291*, 21817−21828.

(16) Kekenes-Huskey, P. M.; Lindert, S.; McCammon, J. A. Molecular basis of calcium-sensitizing and desensitizing mutations of the human cardiac troponin C regulatory domain: a multi-scale simulation study. *PLoS Comput. Biol.* **2012**, *8*, No. e1002777.

(17) Cheng, Y.; Lindert, S.; Kekenes-Huskey, P.; Rao, V. S.; Solaro, R. J.; Rosevear, P. R.; Amaro, R.; McCulloch, A. D.; McCammon, J. A.; Regnier, M. Computational studies of the effect of the S23D/S24D troponin I mutation on cardiac troponin structural dynamics. *Biophys. J.* **2014**, *107*, 1675−1685.

(18) Bowman, J. D.; Lindert, S. Computational Studies of Cardiac and Skeletal Troponin. *Front. Mol. Biosci.* **2019**, *6*, 68.

(19) Siddiqui, J. K.; Tikunova, S. B.; Walton, S. D.; Liu, B.; Meyer, M.; de Tombe, P. P.; Neilson, N.; Kekenes-Huskey, P. M.; Salhi, H. E.; Janssen, P. M. L.; Biesiadecki, B. J.; Davis, J. P. Myofilament

Calcium Sensitivity: Consequences of the Effective Concentration of Troponin I. *Front. Physiol.* **2016**, *7*, 632.

(20) Yamada, Y.; Namba, K.; Fujii, T. Cardiac muscle thin filament structures reveal calcium regulatory mechanism. *Nat. Commun.* **2020**, *11*, 153.

(21) Goodsell, D. S.; Autin, L.; Olson, A. J. Illustrate: Software for Biomolecular Illustration. *Structure* **2019**, *27*, 1716−1720.e1.

(22) Takahashi-Yanaga, F.; Morimoto, S.; Harada, K.; Minakami, R.; Shiraishi, F.; Ohta, M.; Lu, Q.-W.; Sasaguri, T.; Ohtsuki, I. Functional consequences of the mutations in human cardiac troponin I gene found in familial hypertrophic cardiomyopathy. *J. Mol. Cell. Cardiol.* **2001**, *33*, 2095−2107.

(23) Kobayashi, T.; Solaro, R. J. Increased Ca2+ affinity of cardiac thin filaments reconstituted with cardiomyopathy-related mutant cardiac troponin I. *J. Biol. Chem.* **2006**, *281*, 13471−13477.

(24) Yumoto, F.; Lu, Q.-W.; Morimoto, S.; Tanaka, H.; Kono, N.; Nagata, K.; Ojima, T.; Takahashi-Yanaga, F.; Miwa, Y.; Sasaguri, T.; Nishita, K.; Tanokura, M.; Ohtsuki, I. Drastic Ca2+ sensitization of myofilament associated with a small structural change in troponin I in inherited restrictive cardiomyopathy. *Biochem. Biophys. Res. Commun.* **2005**, *338*, 1519−1526.

(25) Zhang, P.; Kirk, J. A.; Ji, W.; Dos Remedios, C. G.; Kass, D. A.; Van Eyk, J. E.; Murphy, A. M. Multiple reaction monitoring to identify site-specific troponin I phosphorylated residues in the failing human heart. *Circulation* **2012**, *126*, 1828−1837.

(26) Trott, O.; Olson, A. J. AutoDock Vina: improving the speed and accuracy of docking with a new scoring function, efficient optimization, and multithreading. *J. Comput. Chem.* **2010**, *31*, 455−461.

(27) Moorthy, A. K.; Singh, S. K.; Gopal, B.; Surolia, A.; Murthy, M. R. N. Variability of calcium binding to EF-hand motifs probed by electrospray ionization mass spectrometry. *J. Am. Soc. Mass Spectrom.* **2001**, *12*, 1296−1301.

(28) *The PyMOL Molecular Graphics System*, Version 2.0; Schrödinger, LLC, 2017.

(29) Warnecke, A.; Sandalova, T.; Achour, A.; Harris, R. A. PyTMs: a useful PyMOL plugin for modeling common post-translational modifications. *BMC Bioinf.* **2014**, *15*, 370.

(30) Phillips, J. C.; Braun, R.; Wang, W.; Gumbart, J.; Tajkhorshid, E.; Villa, E.; Chipot, C.; Skeel, R. D.; Kalé, L.; Schulten, K. Scalable molecular dynamics with NAMD. *J. Comput. Chem.* **2005**, *26*, 1781−1802.

(31) Huang, J.; MacKerell, A. D. CHARMM36 all-atom additive protein force field: validation based on comparison to NMR data. *J. Comput. Chem.* **2013**, *34*, 2135−2145.

(32) Ohio Supercomputer Center. *Owens Cluster*; Ohio Supercomputer Center, 1987.

(33) Hamelberg, D.; Mongan, J.; McCammon, J. A. Accelerated molecular dynamics: a promising and efficient simulation method for biomolecules. *J. Chem. Phys.* **2004**, *120*, 11919−11929.

(34) Huber, G. A.; McCammon, J. A. Browndye: A Software Package for Brownian Dynamics. *Comput. Phys. Commun.* **2010**, *181*, 1896−1905.

(35) Baker, N. A.; Sept, D.; Joseph, S.; Holst, M. J.; McCammon, J. A. Electrostatics of nanosystems: application to microtubules and the ribosome. *Proc. Natl. Acad. Sci. U.S.A.* **2001**, *98*, 10037−10041.

(36) Covalent and Ionic Radii. https://chem.libretexts.org/@go/page/198185 (March 19, 2021).

(37) Wang, D.; Robertson, I. M.; Li, M. X.; McCully, M. E.; Crane, M. L.; Luo, Z.; Tu, A.-Y.; Daggett, V.; Sykes, B. D.; Regnier, M. Structural and functional consequences of the cardiac troponin C L48Q Ca(2+)-sensitizing mutation. *Biochemistry* **2012**, *51*, 4473−4487.

(38) Ainavarapu, S. R. K.; Brujić, J.; Huang, H. H.; Wiita, A. P.; Lu, H.; Li, L.; Walther, K. A.; Carrion-Vazquez, M.; Li, H.; Fernandez, J. M. Contour length and refolding rate of a small protein controlled by engineered disulfide bonds. *Biophys. J.* **2007**, *92*, 225−233.

(39) Berg, J. M.; Tymoczko, J. J.; Stryer, L. Secondary Structure: Polypeptide Chains Can Fold Into Regular Structures Such as the

Alpha Helix, the Beta Sheet, and Turns and Loops. *Biochemistry*, 5th ed.; W H Freeman: New York, 2002; Section 3.3. Available from: https://www.ncbi.nlm.nih.gov/books/NBK22580/ (accessed March 15, 2021).

(40) Wang, X.; Li, M. X.; Sykes, B. D. Structure of the regulatory N-domain of human cardiac troponin C in complex with human cardiac troponin I147−163 and bepridil. *J. Biol. Chem.* **2002**, *277*, 31124−31133.

(41) Bowman, J. D.; Coldren, W. H.; Lindert, S. Mechanism of Cardiac Troponin C Calcium Sensitivity Modulation by Small Molecules Illuminated by Umbrella Sampling Simulations. *J. Chem. Inf. Model.* **2019**, *59*, 2964−2972.

(42) Bowman, J. D.; Lindert, S. Molecular Dynamics and Umbrella Sampling Simulations Elucidate Differences in Troponin C Isoform and Mutant Hydrophobic Patch Exposure. *J. Phys. Chem. B* **2018**, *122*, 7874−7883.

(43) Dewan, S.; McCabe, K. J.; Regnier, M.; McCulloch, A. D.; Lindert, S. Molecular Effects of cTnC DCM Mutations on Calcium Sensitivity and Myofilament Activation-An Integrated Multiscale Modeling Study. *J. Phys. Chem. B* **2016**, *120*, 8264−8275.

(44) Lindert, S.; Kekenes-Huskey, P. M.; McCammon, J. A. Long-timescale molecular dynamics simulations elucidate the dynamics and kinetics of exposure of the hydrophobic patch in troponin C. *Biophys. J.* **2012**, *103*, 1784−1789.